

# Development of High-Temperature Seismometers for Near-Field Microearthquake Monitoring

Nori Nakata<sup>1</sup>, Paul Cook<sup>1</sup>, Avinash Nayak<sup>1</sup>, Chet Hopp<sup>1</sup>, Sireesh Dadi<sup>2</sup>, Ben Wygal<sup>2</sup>, Aleksei Titov<sup>2</sup>

<sup>1</sup>Lawrence Berkeley National Laboratory, <sup>2</sup>Fervo Energy

nnakata@lbl.gov

**Keywords:** Seismic monitoring, High temperature, EGS

## ABSTRACT

High-resolution monitoring of microearthquakes near enhanced geothermal system (EGS) reservoirs is essential for understanding rock-fluid interactions and reservoir evolution during and after stimulation and production. However, the extreme downhole conditions of EGS environments, characterized by high temperatures and pressures, pose significant challenges for conventional seismic and other geophysical sensors.

To address this, we are developing a high-temperature, single-level, three-component seismometer based on a 4.5 Hz string-type geophone with a seven-conductor cable. The mechanical and electrical components have been redesigned to enhance durability under conditions up to 260 degree C and 40 MPa. In July 2025, we deployed the sensor at a depth of 2,132 m (176 degree C) in a vertical borehole at the Cape field, Utah, to continuously monitor reservoir activity and seismicity. The sensor has operated successfully since installation, detecting more than 100 times as many earthquakes as the nearby UU.FORK station at 282 m depth. Even compared with borehole distributed acoustic sensing (DAS) data, our instrument recorded approximately 3-5 times more events, demonstrating superior sensitivity and robustness in high-temperature environments. The sensor is still working (last accessed in January 2026)

## 1. INTRODUCTION

High-resolution seismic monitoring is a critical component of enhanced geothermal system (EGS) development, providing direct and indirect observations of fracture activation, stress redistribution, and fluid-rock interactions during stimulation and production. Microearthquakes generated in EGS reservoirs often occur at very small magnitudes, particularly in well-designed stimulation campaigns aimed at minimizing seismic hazard. Detecting and characterizing such events requires sensors deployed close to the reservoir, where seismic waveforms retain high-frequency content and signal-to-noise ratios are maximized. However, near-field monitoring in EGS environments is technically challenging due to extreme downhole conditions, including elevated temperatures, high pressures, and chemically aggressive fluids, which exceed the operating limits of most conventional seismic sensors.

Recent EGS projects have increasingly targeted higher-temperature reservoirs to improve energy recovery and economic viability, further intensifying the need for robust downhole instrumentation. At depths of several kilometers, temperatures commonly exceed 200 °C, and hydrostatic pressures approach tens of megapascals. While surface networks and shallow borehole stations remain essential for regional monitoring and hazard mitigation, their sensitivity is often insufficient to capture dense microseismicity associated with reservoir-scale fracture processes. Distributed acoustic sensing (DAS) offers valuable spatial coverage, but its sensitivity and interpretability depend strongly on coupling conditions and processing approaches. These limitations highlight the need for durable, high-sensitivity point sensors capable of long-term operation in extreme geothermal environments.

In this study, we present the development, deployment, and performance of a high-temperature, single-level, three-component borehole seismometer designed specifically for near-field microearthquake monitoring in EGS settings. The sensor is engineered to operate at temperatures up to 260 °C and pressures up to 5000 psi, enabling deployment at reservoir-relevant depths. We describe the mechanical design and fabrication of the instrument, its deployment in a deep monitoring well at the Cape geothermal field in Utah, and its noise stabilization behavior following installation. Using continuous recordings acquired during active stimulation, we demonstrate the sensor's ability to detect and characterize microearthquakes at magnitudes well below the detection threshold of nearby surface and shallow borehole stations. Comparisons with conventional sensors and DAS measurements illustrate the complementary role of high-temperature borehole seismometers in advancing seismic monitoring and reservoir characterization for next-generation EGS projects.

## 2. SENSOR DEVELOPMENT

The high-temperature borehole seismometer developed in this study is designed to operate up to 260°C and 5000 psi (34.5 MPa, ~3500 m depth for hydrostatic pressure) of near-field EGS environments. The pressure limit can be changed to higher numbers relatively easily. The sensor housing is fabricated from high-strength metal stock using precision machining to ensure mechanical integrity, dimensional accuracy, and long-term stability at high temperatures. Tight machining tolerances are required to maintain proper alignment of internal components and to accommodate thermal expansion without compromising performance (Figure 1a). Pressure-critical joints are sealed by welding to provide a robust, leak-tight enclosure suitable for downhole deployment (Figure 1b). Prior to final assembly, individual components—including the geophone carrier, internal wiring, and electrical feedthroughs—are prepared and inspected to verify compatibility with high-temperature operation (Figure 1c). The central section of the tool houses a single-level, three-component 4.5 Hz geophone connected through a seven-conductor cable rated for elevated temperatures.

The fully assembled sensor has a total length of approximately 3 m and is configured as a modular tool string optimized for borehole coupling and mechanical stability (Figure 1d). From top to bottom (right to left in the picture), the assembly consists of the geophone package, a mechanical clamping system to ensure firm coupling to the borehole wall, and two weighted sections that stabilize the tool and suppress unwanted motion. This configuration enhances sensitivity to small-magnitude seismic signals by maximizing coupling between the sensor and the surrounding formation while minimizing tool resonance and vibration. The combination of robust mechanical design, high-temperature-rated components, and optimized geometry enables reliable seismic monitoring in extreme geothermal environments where conventional downhole sensors often experience performance degradation or failure.

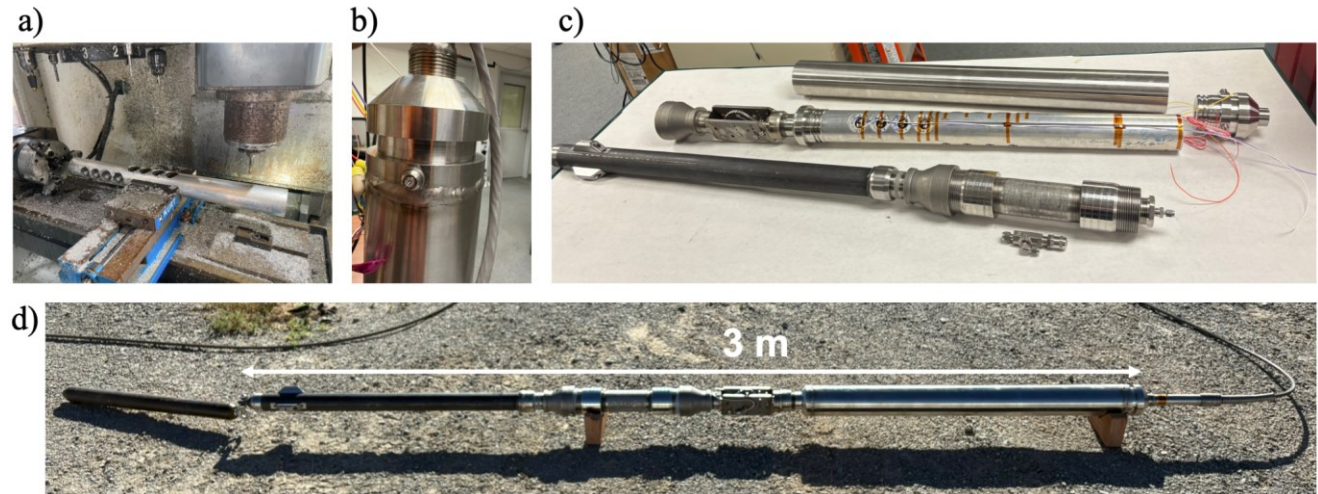


**Figure 1. Sensor manufacturing. (a) Machining of the sensor housing operated by Paul Cook at LBNL. (b) Welded joint. (c) Sensor parts before assembling. The middle part, which houses geophones, will be put inside of the tube shown at the top of the picture. (d) Entire sensor, which is 3 m. From right to left, the geophones, a clamp system, a weight, and another weight.**

### 3. SENSOR DEPLOYMENT

The sensor was deployed in a monitoring well (Delano 1-OB) at the Cape Station geothermal field in Utah on July 27, 2025, in collaboration with Fervo Energy (Figure 2a). A double-clamp deployment technique using a crane was employed to lower the sensor into the well in a cost-effective and controlled manner (Figure 2b). After approximately four hours of deployment, the sensor reached the depth of 2,132 m, where the ambient temperature was measured at 176 °C. The downhole cable was connected to a Reftek RT130 data logger, which transmits the continuous seismic data to an LBNL server for near-real-time data processing and analysis. Initial data acquisition was conducted at a sampling rate of 1000 samples per second (sps), after which the rate was increased to 4000 sps to improve temporal resolution, particularly for detecting and characterizing smaller-magnitude earthquakes.

Following deployment, a stabilization period was required before the sensor reached optimal performance. Elevated noise levels were initially observed, likely due to fluid movement within the borehole, ongoing thermal equilibration, and minor mechanical adjustments of the sensor system. Over time, these effects diminished as the sensor equilibrated with downhole conditions. Notably, it took more than two weeks for the noise level to stabilize, after which the background noise was reduced by nearly two orders of magnitude compared to the initial deployment period (Figure 3). This progressive noise reduction highlights the importance of allowing sufficient settling time for high-temperature borehole sensors before conducting detailed seismic analyses.

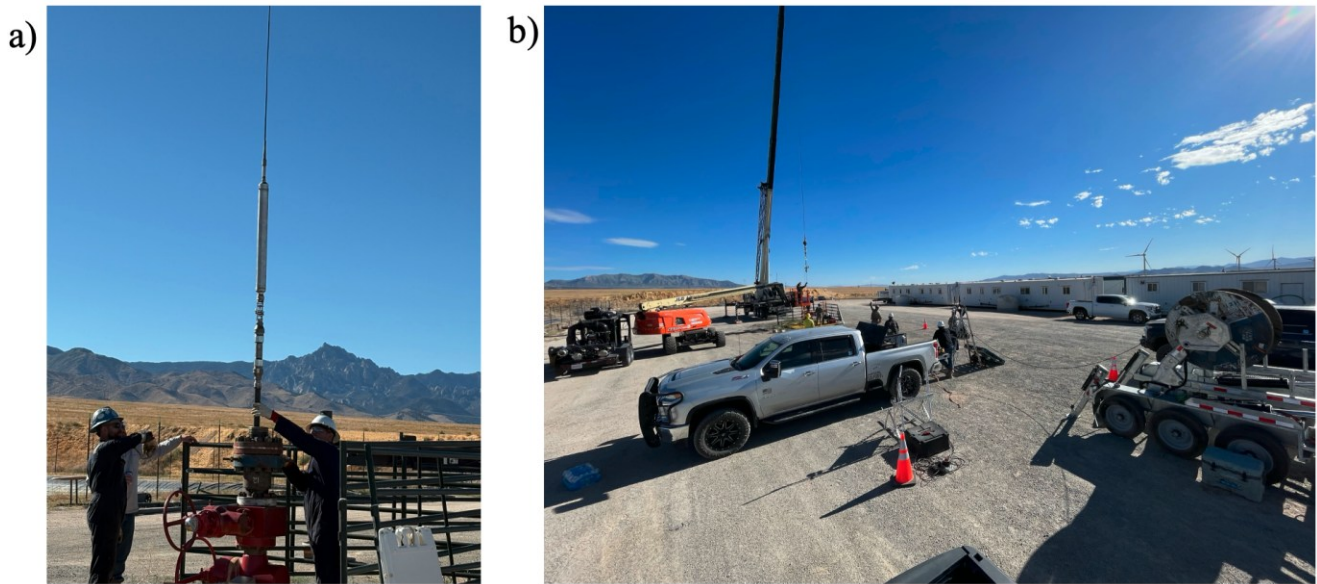


Figure 2. Sensor deployment with a double-clamp technique with a crane. (a) Sensor installing into the well. (b) A photo during the deployment.

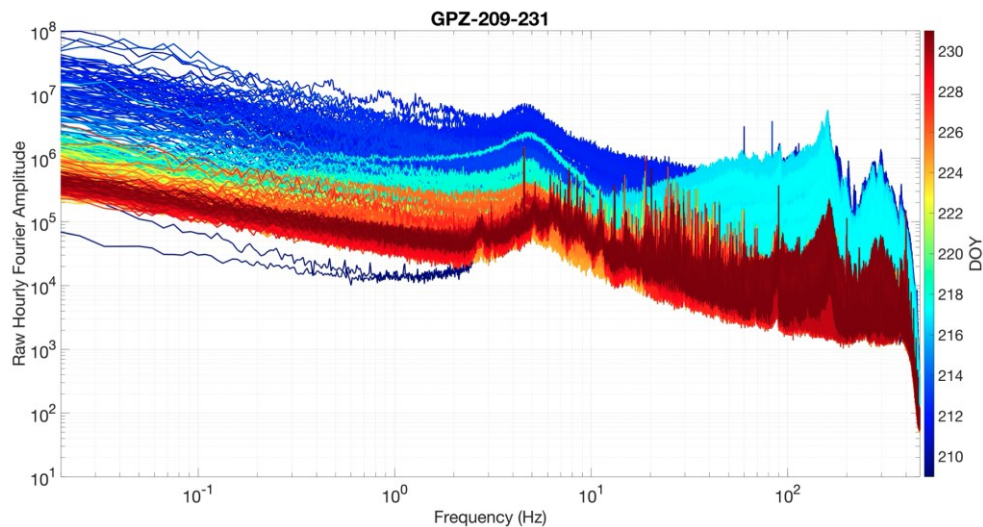


Figure 3. Noise level reduction over 20 days from the deployment on July 28th (Julian day 209).

## 4. RECORDS

### 4.1 Near-Field Microearthquake waveforms

From the beginning of data acquisition through the present, the sensor has continuously recorded high-quality seismic waveforms (Figure 4). Owing to the high sensitivity of the instrument and the active stimulation operations in the field, nearly all transient spikes visible in Figure 4a correspond to earthquake signals rather than noise. A clear increase in the seismicity rate is observed during stimulation periods, consistent with expectations for induced seismicity. The three-component configuration of the sensor provides additional degrees of freedom, enabling not only reliable event detection but also detailed characterization of earthquake waveforms. Note that both P and S waves are recorded over the three components, rather P waves are dominant in the Z component when the sensor is at the surface, due to depths of the sensor and hypocenters, three-component particle-motion analysis can be used to infer wave propagation directions (Sun et al., 2024).

Amplitude spectra of earthquakes spanning a range of magnitudes exhibit systematic amplitude variations and show good agreement with theoretical source spectra (Figure 5). Notably, nearly the entire frequency band of the spectra for earthquakes as small as  $M -1.5$  remains above the background noise level. This highlights the advantage of near-field borehole seismometers for characterizing small-magnitude

events that are often undetectable by surface stations. Such high sensitivity is particularly important for investigating subtle physical processes, including stress changes associated with microearthquake activity and reservoir evolution (Chang et al., 2023).

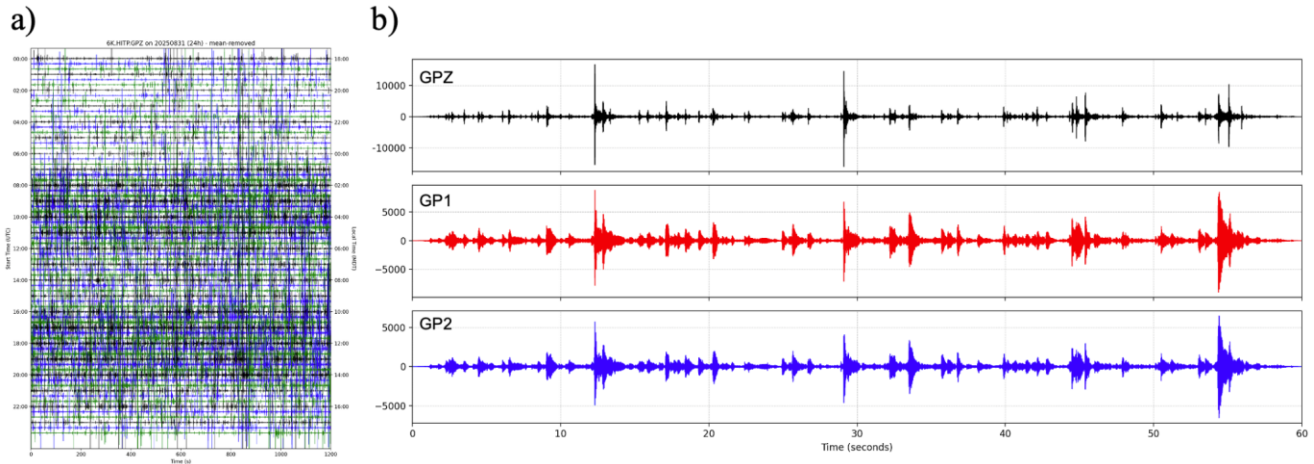


**Figure 4.** Recorded waveforms in the time domain. (a) 24-hour data on August 31, 2025. Each line shows the continuous seismic motion in 20 minutes. Stimulation occurred around 9:00-12:00 and 16:00-19:00. (b) One-minute data in three components. A bandpass filter of 80-160 Hz is applied for visualization purposes. The largest earthquake in this time interval is smaller than M-2.5.

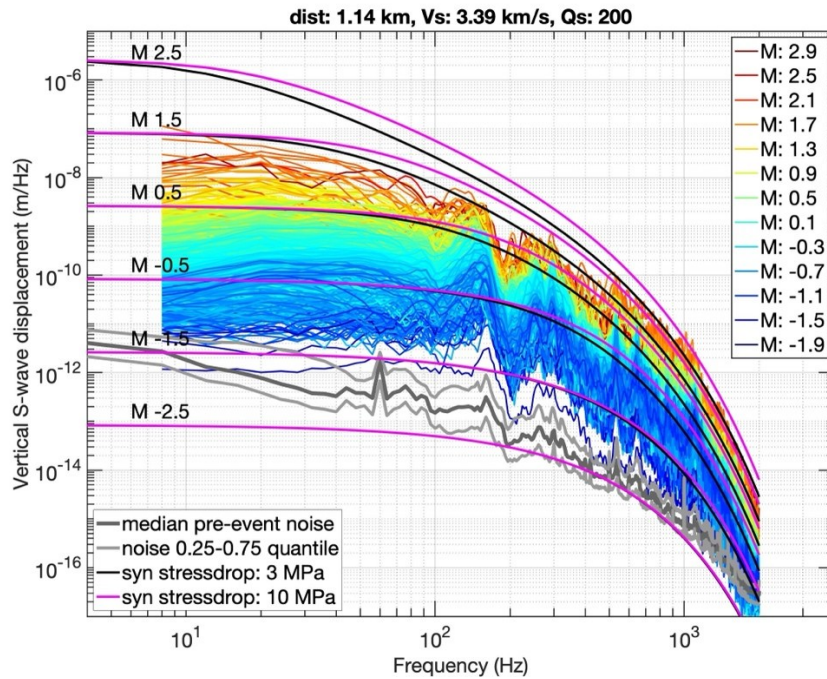


**Figure 5.** Amplitude spectra of recorded earthquake S waves (colored lines), background noise (gray lines), and theoretical spectra at various earthquake magnitudes (black and magenta lines). The theoretical curve is computed based on the distance of 1.14 km, stress drop of 3 MPa, S-wave velocity of 3.39, and quality factor of 200.

#### 4.2 Comparison with other sensors

We compare seismic records from our borehole sensor with those from the UU.FORK station, which is the second deepest seismic sensor in the study area (Figure 6). Larger-magnitude events are clearly observed by both instruments; however, our sensor records a substantially greater number of smaller events. Using a waveform-based detection algorithm based on autocorrelation, our sensor detects more than 100 times as many earthquakes as UU.FORK. Assuming a Gutenberg–Richter b-value of approximately 1, this detection improvement corresponds to nearly two orders of magnitude enhancement in magnitude completeness.

We also compare our borehole recordings with distributed acoustic sensing (DAS) data acquired in the Delano 1-OB and Gold wells (Figure 7). The largest event in Figure 7a, occurring at approximately 1 s, is clearly observed in the DAS data, whereas subsequent smaller events are less distinctly resolved. Because DAS data can be processed using array-based techniques to enhance signal-to-noise ratio, a direct comparison of detection sensitivity between DAS and point sensors is not straightforward. Nevertheless, the high resolution and precision of deep high-temperature seismometer measurements provide, even though it is a single sensor, valuable constraints for accurate magnitude estimation and source characterization.

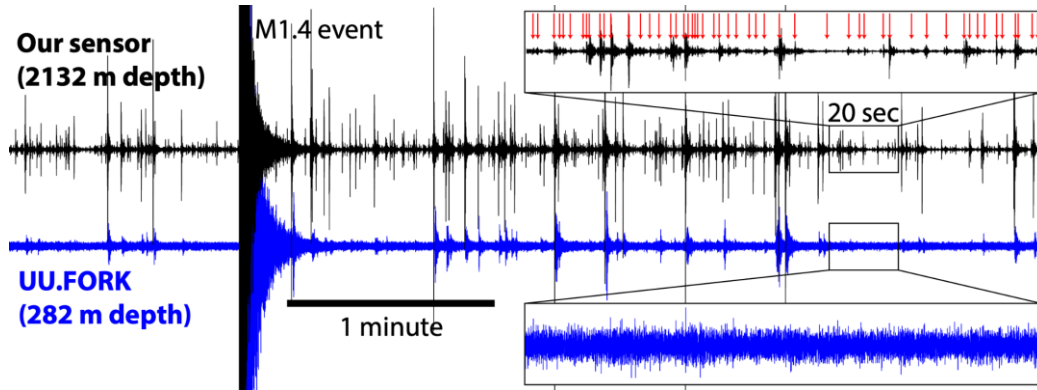


**Figure 6.** Comparison of waveforms between our sensor (black) and the 2nd deepest sensor in the area, UU.FORK (blue) over 5 minutes. The magnitude of the largest-amplitude event is 1.4. The insets show the detailed waveforms within the 20 seconds highlighted by the black boxes. The red arrows indicate the detected events using a waveform-based detection algorithm.

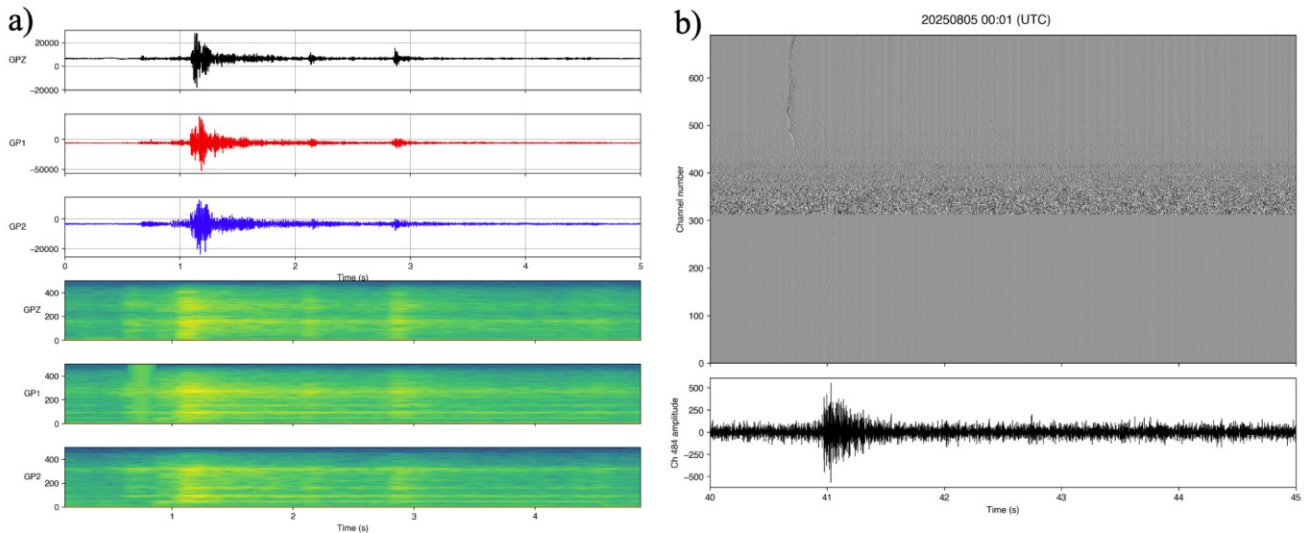


**Figure 7.** Comparison of waveforms between (a) our sensor and (b) DAS in the Gold well (closer to the earthquake source: channels larger than 315) and the 1-OB well (which hosts our sensor: channels smaller than 315). In panel (a), amplitude spectrograms computed by short-time Fourier transform are shown in the bottom three sub-panels. In panel (b), the bottom sub-panel shows the waveform recorded by a DAS receiver, which is the closest to our sensor.

## 5. EARTHQUAKE DETECTION

We apply the high-temperature borehole seismometer data to both earthquake characterization and the detection of small-magnitude events. Using cataloged events, the extracted waveforms exhibit clear P- and S-wave arrivals, often accompanied by at least two distinct reflected phases (Figure 8a). These reflected phases are likely generated at major impedance contrasts, such as the top of the granitoid basement and the ground surface. The high signal quality and repeatability of the recorded waveforms enable detailed waveform similarity analysis. Clustering of the earthquakes reveals well-defined waveform families, providing important constraints on fracture geometry and activation patterns within the reservoir (e.g., Nakata et al., 2025).

Building on these results, we select 20 high-quality waveforms from Figure 8a as templates and apply a template-matching approach to detect smaller, previously uncataloged events. While post-processing is required to remove false detections and ensure event quality, this approach substantially enhances detection capability. Over a 2.5-month period, more than 200,000 events are identified, demonstrating the exceptional sensitivity of the near-field high-temperature seismometer for resolving dense microseismicity. These results highlight the potential of template-based detection combined with robust borehole instrumentation to significantly improve seismic monitoring and fracture characterization in high-temperature EGS environments.

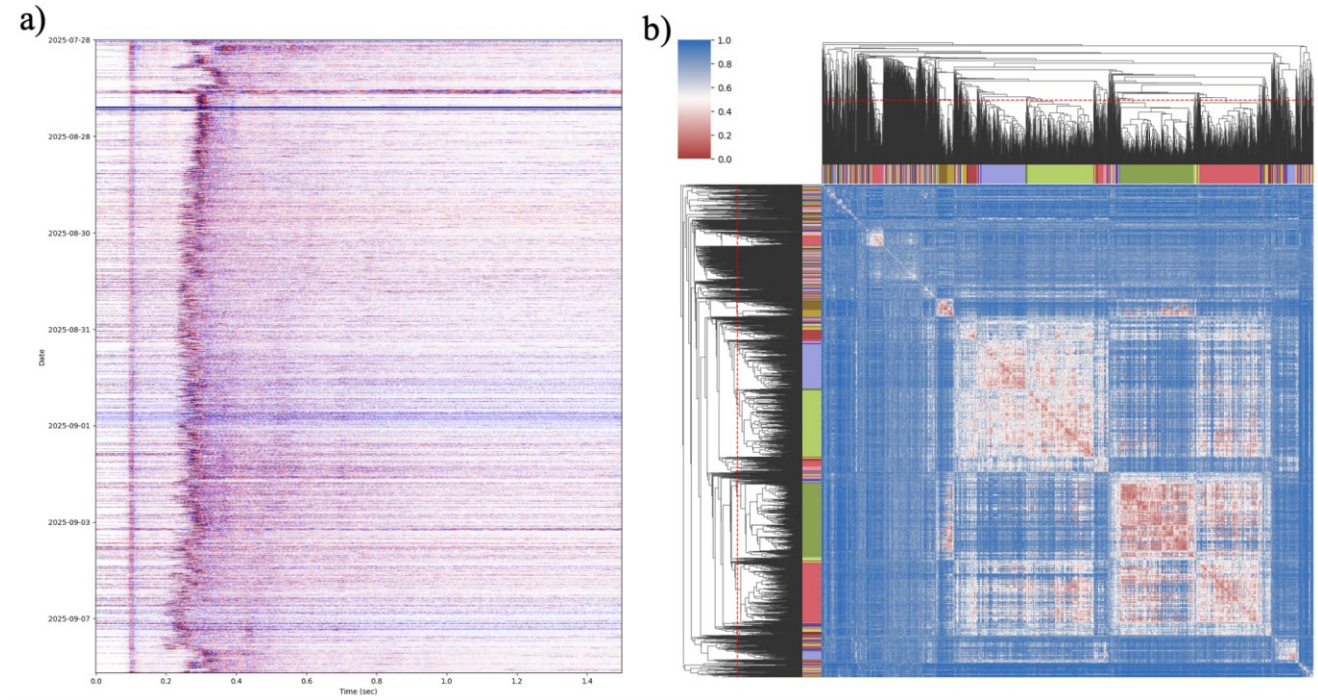


**Figure 8. (a) Earthquake waveforms recorded by our sensor, aligned by the P-wave onset time, which is at 0.1 s in the plot. The largest amplitude phase is the direct S wave. (b) Earthquake clustering of the waves shown in Panel (a).**

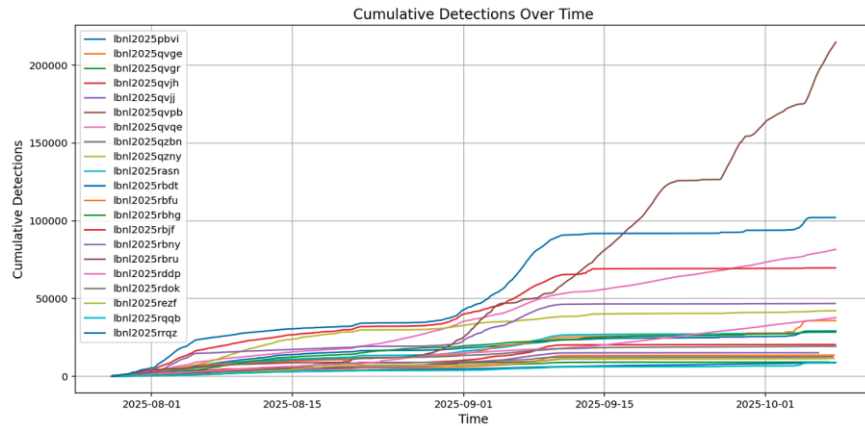


**Figure 9. Detected earthquakes using template matching. Each line represents detections using one template.**

## 6. CONCLUSIONS

We have developed and successfully deployed a high-temperature, three-component borehole seismometer designed for near-field microearthquake monitoring in EGS environments. The sensor has operated reliably at a depth of 2,132 m and a temperature of 176 °C, demonstrating stable long-term performance following an initial noise stabilization period. Continuous recordings reveal high-quality seismic waveforms, clear increases in seismicity rate during stimulation, and amplitude spectra that remain above the noise level even for earthquakes as small as M-1.5. Compared with nearby shallow borehole stations, the sensor detected more than two orders of magnitude more events, underscoring the importance of deep, near-field monitoring for resolving small-magnitude seismicity.

Template matching and waveform clustering further demonstrate the potential of high-temperature borehole sensors for detailed earthquake characterization and fracture analysis. Over a 2.5-month period, more than 200,000 events were detected, revealing dense microseismic activity that would otherwise remain unobserved. These results highlight the critical role of robust downhole instrumentation in future EGS developments, particularly as stimulation strategies continue to reduce seismic hazard while pushing detection requirements

toward lower magnitudes. High-temperature borehole seismometers, used in combination with surface networks and DAS, offer a powerful and complementary approach for advancing seismic monitoring, reservoir characterization, and the safe development of geothermal energy resources.

## 7. ACKNOWLEDGMENT

This work was supported by the U.S. Department of Energy, Hydrocarbons and Geothermal Energy Office, under Award Number DE-AC02-05CH11231 with Lawrence Berkeley National Laboratory. We thank Fervo Energy for letting us to deploy the sensor and share the results.

## REFERENCES

- Chang, H., Abercrombie, R. E., Nakata, N., Pennington, C. N., Kemna, K. B., Cochran, E. S., & Harrington, R. M. (2023). Quantifying site effects and their influence on earthquake source parameter estimations using a dense array in Oklahoma. *Journal of Geophysical Research: Solid Earth*, 128, e2023JB027144
- Nakata, N., H. Chang, S.-M. Wu, Z. Bi, L.-W. Chen, F. Soom, H. Gao, A. Titov, and S. Dadi (2025) Fracture Characterization and Stress Communication Revealed by Induced Seismicity at the Cape Modern Geothermal Field, Utah, *GRC Transactions*, 49, 2025, 1191-1202.
- Sun, J., Y. Mukuhira, T. Nagata, T. Nonomura, M. C. Fehler, H. Moriya, N. Nakata, and T. Ito (2024) P-S travel-time detection and hypocenter location of low-SNR events using polarization in the time-frequency domain, *Bulletin of the Seismological Society of America*, 114 (5), 2359-2375.